Journal of Chromatography A 1760 (2025) 466245

Contents lists available at ScienceDirect

Journal of Chromatography A

journal homepage: www.elsevier.com/locate/chroma

Integration of capillary chromatography columns into a 3D-printed microfluidic multiport valve for miniaturized multi-column chromatography

Juliane Diehm, David Achauer, Matthias Franzreb *

Institute of Functional Interfaces, Karlsruhe Institute of Technology, 76344 Eggenstein-Leopoldshafen, Germany

ARTICLE INFO

Keywords:
Monolithic capillary columns
Continuous chromatography
Small-scale chromatography
Multi-column chromatography
Miniaturization

ABSTRACT

Driven by the need for smaller and more efficient continuous chromatographic systems, this study explores the feasibility of miniaturizing multi-column chromatography by integrating monolithic capillary columns directly into a 3D-printed valve rotor. First, monolith capillary ion-exchange columns were synthesized in PEEK capillaries with a diameter of 0.75 mm and a 3D-printed rotor system that can hold these capillary columns was developed. Single-column experiments confirm that the synthesized monolithic columns can separate the proteins hemoglobin and lysozyme with step elution, although the dynamic binding capacity is significantly lower than that of commercial equivalents. Subsequent multi-column tests reveal that a standard gradient simulated moving bed (SMB) approach faces limitations due to elevated back pressure of the columns, resulting in leakages. To overcome this issue, a continuous multi-column chromatography (CMCC) setup was implemented, enabling promising separations with more than 60% yield and 80% purity for both proteins with switching intervals as low as 30 s, allowing for a fast response time of the system. Although further improvements in monolith morphology, functionalization, and valve sealing are needed, these findings highlight the potential of integrating monolith columns in miniaturized multi-column processes.

1. Introduction

Continuous manufacturing has gained increasing attention in the biopharmaceutical industry due to its potential to produce more product in less time and at lower cost compared to traditional batch processes [1–3]. Chromatography, as one of the most frequently applied unit operations in downstream processing (DSP), plays a central role in this development [1,4]. However, the implementation of continuous processing in biopharmaceutical manufacturing remains limited [5], despite numerous case studies highlighting its advantages [6–8].

Two major challenges for the implementation of continuous processes are the lack of readily available scale-down equipment, which leads to a high material and product consumption during process development [5], and the availability of reliable process analytics. In continuous manufacturing, process analytical technology (PAT) is essential for ensuring consistent product quality via real-time monitoring and active process control [9]. However, commonly used PAT tools typically exclude established off-line analytical techniques, such as high-performance liquid chromatography (HPLC) or mass spectrometry (MS), due to their long analysis times and extensive sample preparation requirements [10].

Despite these limitations, HPLC and MS could play a crucial role in monitoring critical quality attributes (CQAs), especially in the context of real-time release testing [11]. Miniaturized systems offer a promising solution by reducing analysis times and material requirements, thus making these high-resolution methods more accessible for PAT applications [5].

To address these challenges, we previously developed a microscale simulated moving bed (μSMB) system featuring a custom 3D-printed central valve. Simulated moving bed chromatography (SMB) is a well-established continuous separation process [12,13], typically used in preparative production processes. With a downscale to feed flow rates of 15 μL/min and column volumes below 353 μL, we successfully demonstrated the suitability of the SMB principle for PAT applications, e.g., in combination with mass spectrometry [14], as well as the applicability of the μSMB system for process development due to its low material consumption [15].

Although significantly smaller than commercial lab-scale SMB systems, the μSMB platform still remains larger than miniaturized analytical-scale single-column chromatography systems. In microcolumn liquid chromatography, columns with diameters below 1 mm are generally used [16], which enables efficient handling of small sample volumes and minimizes sample dilution when operated at low flow rates, thus enhancing measurement sensitivity [17].

* Corresponding author.
E-mail address: matthias.franzreb@kit.edu (M. Franzreb).

https://doi.org/10.1016/j.chroma.2025.466245
Received 29 April 2025; Received in revised form 20 July 2025; Accepted 22 July 2025
Available online 14 August 2025

This raises the question of how far multi-column chromatography systems can be miniaturized. A major limiting factor is extra column volume (ECV), which contributes to band broadening and degrades separation performance [18]. In industrial SMB systems, the band broadening effects of the extra column volume are often not significant and can be accounted for during process point determination using simple models that consider the additional retention time and adjust the flow rates and switching time accordingly [18,19]. However, upon downscaling, column volumes decrease rapidly (e.g., halving the diameter reduces volume by a factor of four), potentially making ECV comparable in magnitude to the column volume. Therefore, reducing ECV in tandem with column miniaturization is essential.

A straightforward strategy for reducing the ECV of the μSMB system is to integrate chromatography columns directly into the 3D-printed central valve. This integration alone, without modifying other system components, reduces the ECV of the setup by 48% just by eliminating the capillaries connecting the columns to the valve.

We explored different ways to directly integrating chromatography columns into the valve and present the most promising approach – a design featuring monolithic capillary columns embedded in the valve body – in this study. While previous μSMB work using external chromatography column housings focused on size-exclusion chromatography, this setup employs ion-exchange chromatography (IEX), due to the complexities associated with synthesizing monoliths with defined pore size distributions. We compare the separation performance of lysozyme and hemoglobin using a gradient SMB setup and an alternative continuous multi-column chromatography (CMCC) process in which the typical IEX process steps (binding, washing, elution, and re-equilibration) are performed in parallel.

2. Material and methods

2.1. Chemicals

Acetone, azobisisobutyronitile (AIBN), blue dextran, cyclohexanol, 1-dodecanol, ethylene glycol dimethylacrylate (EGDMA), glycidyl methacrylate (GMA), hemoglobin, iminodiacetic acid (IDA), methanol, sodium hydroxide, and sodium chloride were purchased from Sigma Aldrich (St. Louis, US). Lysozyme was obtained from AppliChem (Darmstadt, DE), potassium phosphate from Carl ROTH (Karlsruhe, DE), and sulfuric acid from Merck (Darmstadt, DE). All chemicals were used without further purification.

2.2. Monolithic column synthesis

The procedure for the in situ polymerization of the monolith structure in polyether ether ketone (PEEK) capillaries was adapted from Sýkore et al. [20]: A mixture of 24% GMA, 16% EGDMA, 6% dodecanol, and 54% cyclohexanol, with 4 mg AIBN per mL mixture, was used for monolith synthesis. The mixture was filled in PEEK capillaries with a diameter of 0.75 mm and a length of 30 cm and sealed at both ends. While PEEK capillaries are uncommon in situ polymer monolith synthesis, they were selected for their flexibility, which facilitates integration into the 3D-printed valve system, unlike stainless steel or fused-silica capillaries. The temperature-induced polymerization process was carried out in an oven (FD 23, Binder, Tuttlingen, DE) at 55 ° C for 12 h. Afterwards, the porogens were removed by flushing the monolith with methanol at 50 μL/min, using syringe pumps (Nemesys M, Cetoni, Korbußen, DE). The functionalization process of the monolith with carboxyl groups for weak cation-exchange chromatography was adapted from Conti et al. [21]: The capillaries were rinsed with water and filled with 2.0 M IDA solution, resulting in the covalent coupling of IDA to the methacrylate backbone via the epoxy group. The capillaries were sealed again and heated at 55 ° C for 72 h. Excess IDA was flushed out with water at 50 μL/min, and the capillaries were stored in water for 72 h. Finally, any remaining unfunctionalized epoxy groups were hydrolyzed with 0.1 mM sulfuric acid at 55 ° C for 24 h.

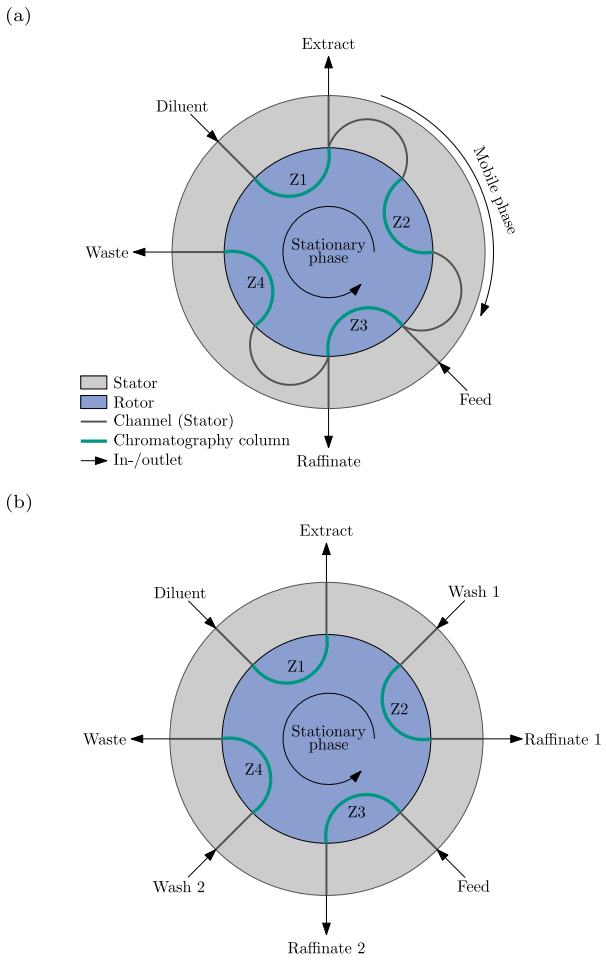

Fig. 1. Connection schematics for the SMB (a) and CMCC (b) setup including in-/outlets connected to the 3D-printed valve stator, channels in the stator, and capillary chromatography columns integrated into the valve rotor. Z1 – Z4: Zone I – Zone IV.

2.3. Monolith characterization and single-column experiments

Single-column experiments were performed with an ÄKTA Pure Chromatography System (Cytiva, Uppsala, SE) using a 19 cm long monolithic capillary (83.9 μL column volume). To determine column porosity, 7.5 μL of non-interacting tracer molecules of different sizes (1 g/L blue dextran and 1% (v/v) acetone [22]) were injected at a flow rate of 50 μL/min, with 20 mM phosphate buffer (pH 6.4) as the mobile phase. For comparison, the same tracer experiment was conducted using an empty capillary instead of the monolith column.

Adsorption experiments were carried out with a feed solution containing 1 g/L hemoglobin and 1 g/L lysozyme. First, 7.5 μL of feed were injected at a flow rate of 50 μL/min with 20 mM phosphate buffer (pH 6.4, buffer A) as mobile phase. The buffer was changed to a 20 mM phosphate buffer with 1 M NaCl (pH 6.4, buffer B) 200 μL after injection for step elution. In another experiment, the elution strength of buffer B was increased in increments of 100 mM NaCl from 0 to 1 M to determine the required elution strength of buffer B. Furthermore, 50 μL of the feed solution was injected into the column at a mobile phase flow rate of 50 μL/min with buffer A as mobile phase, in order to determine the DBC of the stationary phase.

2.4. Multi-column chromatography experiments

Four monolith ion-exchange columns with an inner diameter of 0.75 mm and a length of 50 mm (column volume of 22.1 μL) were used

Table 1
Process parameters of the SMB experiment.

Run	Zone flow in CVS				Flow rate in µL/min					t_s in s	pH
	Zone I	Zone II	Zone III	Zone IV	Diluent	Extract	Feed	Raffinate	Waste		
SMB	2	0.95	1.54	1	33.79	17.74	10	9.15	16.9	30	6.4

Table 2
Process parameters of the CMCC experiments.

Run	Zone flow in CVS				Flow rate in µL/min				t_s in s	pH
	Zone I	Zone II	Zone III	Zone IV	Eluent	Wash	Feed	Re-equilibration		
CMCC 1	2	2	0.59	2	33.8	33.8	10	33.8	30	6.4
CMCC 2	2.66	2.66	0.59	2.66	45	45	10	45	30	6.4
CMCC 3	2.66	2.66	0.59	2.66	45	45	10	45	30	7.4
CMCC 4	4.73	4.73	0.59	4.73	40	40	5	40	60	7.4
CMCC 5	2.66	2.66	0.59	2.66	45	45	10	45	30	8.2

for all multi-column experiments. Besides the changes in the valve and the chromatography columns, the general SMB setup was as described in previous studies [15], except that syringe pumps (Nemesys S, Cetoni, Korbußen, DE) were used as flow source instead of the microfluidic flow controller. The feed solution contained 0.5 g/L of each protein (lysozyme and hemoglobin) dissolved in 20 mM phosphate buffer at various pH levels. To increase the elution strength of the diluent, 600 mM NaCl were added to the respective phosphate buffer.

Besides the open-loop four zone SMB process, a different CMCC process was evaluated, where the different steps of typical elution chromatography (binding, washing, elution, re-equilibration) were carried out in parallel in separate columns. The syringe pumps were connected to the diluent, extract, feed, and raffinate streams in SMB mode for flow generation, and to all inlets (diluent, wash1, feed, wash2) in CMCC mode (see Fig. 1). The remaining outlet streams were collected in 1.5 mL centrifuge tubes (Eppendorf, Hamburg, DE). Apart from that, only the stator's connection channels were changed between the SMB and CMCC setups, while all other components of the valve system remained the same. Fig. 1 schematically depicts the connections in the valve in both setups. For better clarity, the contact surface between rotor and stator is shown in a radial view, although in reality it is axial.

A classic SMB setup consists of four zones; here, one column per zone was used. The columns are periodically switched one position against the flow direction of the mobile phase, thereby simulating a countercurrent between the mobile and stationary phases. This allows for a continuous separation of a feed stream into two fractions: the raffinate and the extract. The less strongly interacting component is recovered in the raffinate, while the more strongly interacting component is recovered in the extract. Each of the zones serves a specific purpose, which is achieved by precisely adjusting the flow rates in the respective zones relative to the switching time of the columns: Zone I is responsible for regenerating the stationary phase, zones II and III for separating the components, and zone IV for regenerating the mobile phase [13,23]. The SMB setup used here had two deviations from the classic SMB implementation: First, the mobile phase leaving zone IV was discarded as waste rather than recycled as diluent, as doing so would require a recycle pump and significantly increase the ECV. The higher mobile phase consumption is negligible at the process scale used. Second, a so-called gradient-SMB method was employed [13], meaning the composition of the mobile phase differs between the diluent and the feed. As a result, in zone I, the interactions of the more strongly interacting component with the stationary phase are reduced, resulting in the elution into the extract.

While in the SMB setup all columns are connected to enable the countercurrent principle between the stationary and mobile phases, the alternative CMCC setup operated the columns in parallel. In zone III, the column was loaded with the feed, so that the more strongly interacting component (lysozym) was adsorbed, while the less strongly interacting component (hemoglobin) flowed through. In zone II, a wash step with the low-salt buffer was performed to flush all unbound hemoglobin from the column. Then, in zone I, lysozyme was eluted from the column using the high-salt buffer, before the column was re-equilibrated in zone IV with the low-salt buffer. Again, the sequence of steps was carried out by switching the column positions through the valve rotor.

A detailed description of the valve design is provided in the next section. Table 1 summarizes the chosen flow rates and column switching time for the SMB process, and Table 2 summarizes those for the CMCC processes. Except for CMCC 1 and 2, experiments were performed in triplicate. For easier comparison, flow rates are given both as absolute values in µL/min and as column void volume per switching interval (CVS). A switching time of 30 s was chosen for most experiments to achieve rapid response times.

Following each run, protein concentrations in the different streams were determined with UV/Vis spectroscopy using a Tecan Spark plate reader (Tecan Group, Männerdorf, CH). The total protein concentration was determined at a wavelength of 280 nm, while the hemoglobin concentration was measured at 405 nm. Lysozyme concentration was calculated by subtracting the hemoglobin concentration from the total protein concentration. The required calibration curves are summarized in Tables S1-S3 in the supplementary information. Additional blank runs without protein in the feed solution were performed to determine blank absorption values for the different streams to eliminate possible interference of leached IDA with the UV measurements.

2.5. 3D-printed valve system

3D printing was chosen as the fabrication method for the valve system because it allows for rapid adaptation and production of various prototypes, including the realization of complex channel geometries. All valve components were 3D-printed using an Asiga Pro 4K65 printer (Asiga, Alexandria, AU). PlasGray (Asiga, Alexandria, AU) and Loctite® 3D 5015 (Henkel, Düsseldorf, DE) were employed as printing materials.

The general valve concept is an axially compressed rotor–stator system, as described previously [24]. However, several modifications were made to integrate the capillary columns directly into the rotor, dividing it into two parts: the main part (rotor part 1) includes capillary holders and the rotor-stator interface (Fig. 2(b)), while rotor part 2 keeps the capillaries in place during experiments and includes a coupling adapter to the motor shaft (Fig. 2(c)).

Because both the inlet and outlet of each capillary column must be located at the rotor-stator interface, the columns are integrated in a curved configuration, as shown in Fig. 2(a). Rotor part 1 contains bores sized for the capillaries and consists of two printing materials: PlasGray in the upper region for mechanical stability, and Loctite® 3D 5015 in the lower region. The elastomeric Loctite material secures the capillaries via a press fit and simultaneously seals the gap between capillary and rotor. The transition between these two printing materials is marked with a black line (5) in Fig. 2(b). Loctite® 3D 5015 is also used to print O-ring-like structures on the sealing surface of the

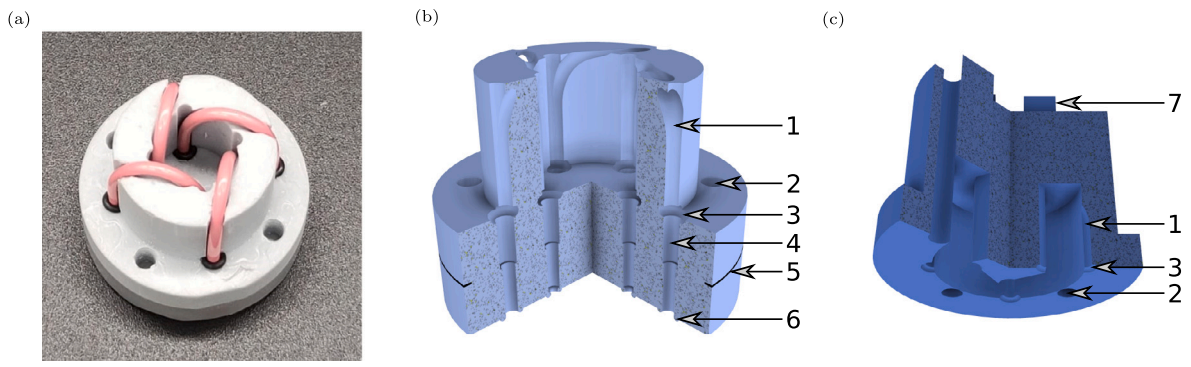

Fig. 2. (a) 3D-printed rotor (part 1) with inserted capillaries. (b) Section view of rotor part 1 CAD; (c) section view of rotor part 2 CAD. 1 – Guide structure for capillaries; 2 – bore for securing rotor part 1 and 2; 3 – O-ring groove; 4 – capillary holder; 5 – height of material change; 6 – O-ring like structures for sealing the rotor-stator interface; 7 – adapter for motor coupling.

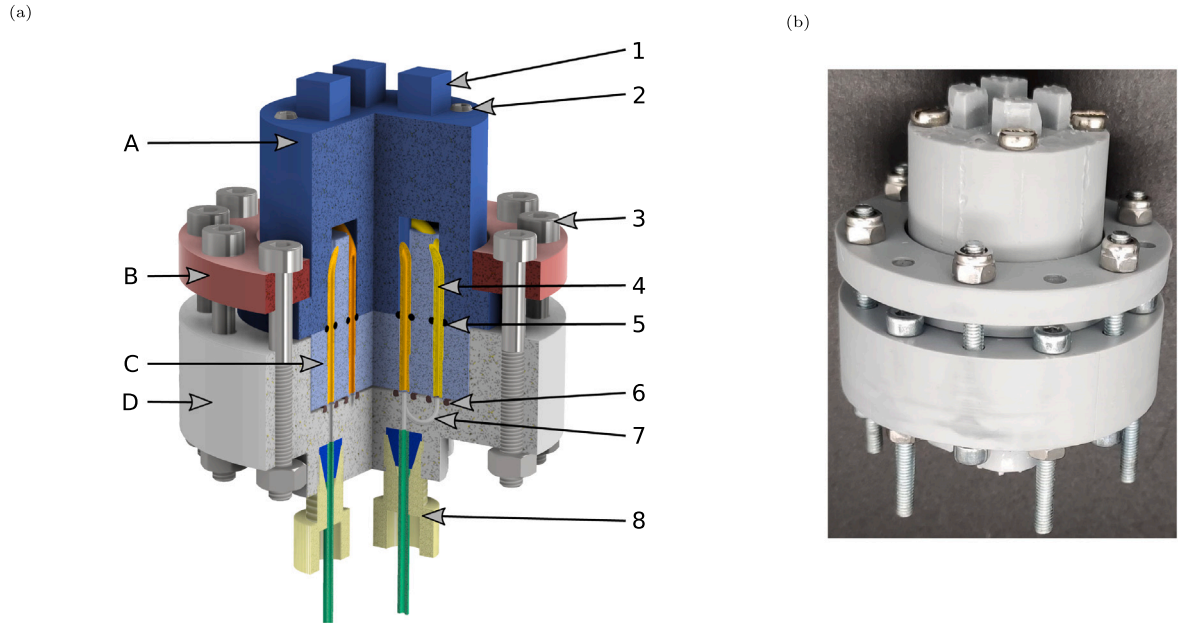

Fig. 3. (a) Section view of the assembled valve system CAD: A – Rotor part 2 (dark blue); B – cover (red); C – rotor part 1 (light blue); D – stator (gray); 1 – adapter for motor coupling; 2 – screw for joining the two rotor parts; 3 – screw for axial compression of rotor and stator; 4 – capillary chromatography column (different shades of yellow/orange indicate the three different visible columns); 5 – O-ring to prevent fluid bypass around the columns; 6 – O-rings sealing the rotor-stator interface; 7 – connection channels in the stator; 8 – fluidic connection (in/outlet) to the stator. (b) Assembled 3D-printed valve system. (For interpretation of the references to color in this figure legend, the reader is referred to the web version of this article.)

rotor (6), both to enhance system tightness and to keep the capillaries in place. The capillaries are inserted into the rotor from the outer bores, the O-ring like structures of the inside bores have a smaller diameter, preventing the capillary from pushing out of the rotor surface on the other side. Alternatively, a steel mesh secured by a self-adhesive polytetrafluoroethylene (PTFE) film (Hightechflon, Konstanz, DE) can serve a similar function. Both rotor parts have guiding structures (1) for the bent capillaries and contain a groove for another O-ring that seals the space between the rotor parts.

With this new design, there are no external fluidic connections on the valve's rotor, which enables to decrease the distance between the in- and outlets of the columns from 10 mm in the previously introduced design to 5 mm, reducing the stator's connection channel volume from 7.3 µL to 4.6 µL and hence minimizing dispersion effects in the system. Details on the channels' geometry can be found in the supplementary material, alongside technical drawings for all the 3D-printed parts (Figures S1-S5). A detailed explanation of the ECV reduction in the valve system resulting from the integrated chromatography columns is provided in Figure S6. With the exception of rotor part 1, all other valve components were printed with PlasGray.

A sectional CAD view of the assembled valve with inserted capillary columns is shown in Fig. 3(a). The flow path from the external fluidic ports (8), through the stator channels (7), and into the capillaries (4) aligns smoothly to reduce turbulences in the transition from one part to the other. Switching from the shown SMB to the CMCC layout requires changing only the stator's connection channels and fluidic ports; all other parts remain the same. Fig. 3(b) shows the fully assembled valve system.

3. Results and discussion

3.1. Single column characterization

Fig. 4(a) depicts the results of the tracer experiments with acetone and blue dextran comparing the monolith column to an empty capillary. All peaks exhibit tailing, but because tailing is also observed in the empty capillary, it is likely due to the laminar flow profile in the overall system rather than an inherent property of the monolith. The influence of the laminar flow profile is especially prominent in the empty capillary, where peak splitting can even be observed for

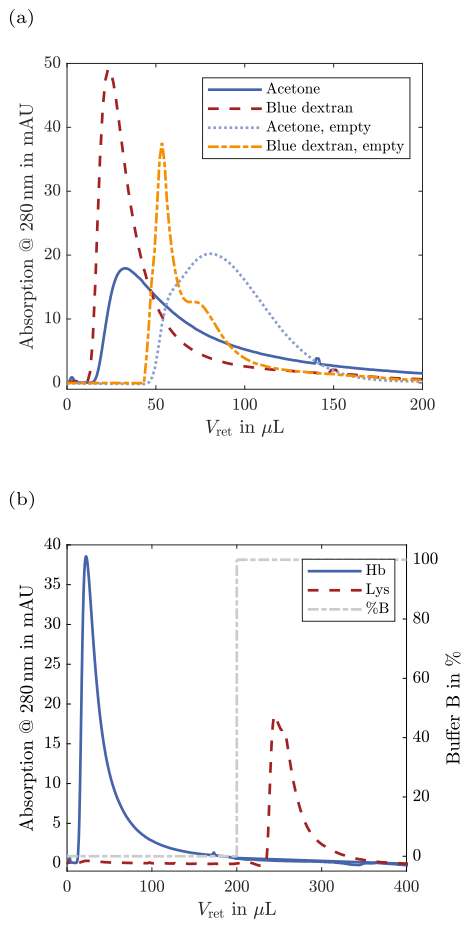

Fig. 4. (a) Tracer experiments with the monolith column vs. an empty capillary. (b) Single-column experiment for the separation of lysozyme and hemoglobin with step-gradient elution. Hb – hemoglobin; Lys – lysozyme.

acetone, besides its comparable low molecular weight. This effect is not observable for the monolith column, suggesting more plug-flow like behavior in the monolith.

Retention times are shorter with the monolith in comparison to the empty capillary, as the solid phase reduces the accessible void volume. From the retention time of acetone, an overall column porosity ε_T of 0.41 can be calculated by multiplying the retention time with the volumetric flow rate divided by the column volume [22]. Since 60% porogen was used in the monomer mixture, some porogen likely remained trapped in non-accessible pores during polymerization. The retention time of blue dextran can be used to determine a theoretical interstitial porosity according, describing the amount of large pores that can be accessed by blue dextran. The resulting value of 0.29 indicates that approximately 70% of the total pore volume consists of large pores, resulting in relatively low surface area and limited binding sites for proteins.

Despite this, the monolith can separate lysozyme from hemoglobin, as shown in Fig. 4(b). Hemoglobin does not bind and elutes with the flow-through, whereas lysozyme is only recovered from the column after switching to the elution buffer. The elution profile of hemoglobin is similar to that of blue dextran, indicating that only the larger fraction of the pores is accessible to the protein. A subsequent experiment with stepwise increase of the elution strength of the mobile phase showed that a NaCl concentration of 600 mM is sufficient to fully elute lysozyme, hence this concentration was used in the multi-column experiments.

In another experiment, a larger lysozyme load was injected into the column to record the breakthrough curve and determine the dynamic binding capacity (DBC) of the monolith, which was 0.88 mg lysozyme per mL solid phase. This is much lower than commercially available ion-exchange monoliths (DBC of 20 mg/mL [25,26]), or other self-synthesized monolithic ion-exchange materials reported in literature (e.g. 5–16 mg/mL [21,27]). The reduced capacity likely stems from the limited surface area due to inhomogeneous pore structure or incomplete functionalization. In literature various protocols to synthesize monoliths with various morphologies and functionalizations exist [28] and although there is substantial room for optimization, this work aims to demonstrate the feasibility of integrating monoliths into the 3D-printed valve system rather than optimizing the monolith itself. Given that these columns can separate low-concentration protein mixtures, it was decided to test them in multi-column experiments despite their low DBC.

3.2. Multi-column chromatography

The system was first evaluated under gradient SMB conditions at pH 6.4. Fig. 5(a) shows that both lysozyme and hemoglobin were recovered in all outlet streams at similar proportions, indicating no effective separation. Additionally, most of both proteins was measured in the raffinate, suggesting insufficient binding of lysozyme. Throughout the experiment, leakages could be observed at the sealing surface between rotor and stator, resulting in an overall volume balance of only 81.2% (±1.7%, n = 3) and a protein mass balance of 53.3% (±2.1%, n = 3) for lysozyme and 55.7% (±1.9%, n = 3) for hemoglobin. Interestingly, the leakages were not evenly distributed among all streams. This was caused by the multiple screws used to compress the rotor and stator, which result in slightly uneven pressure across the sealing surface and thus lead to leakage in specific inlet or outlet streams. This effect is probably enhanced by the comparably high back pressure resulting from connecting the monolith columns in series in comparison to the back pressures of previously used chromatography columns (3 bar compared to 0.2 bar at 50 µL/min). To address this, future studies could reduce leakage by modifying the compression mechanism to ensure uniform pressure across the entire sealing surface.

The observed leakage leads to deviation in the zone flow rates from the desired process point, resulting in an insufficient separation. Especially the flow rate in zone IV was much lower as expected, since all leakages accumulated to that point, resulting in a higher salt concentration in zone IV which is directly transferred to zone III after switching. Hence, the binding of lysozyme to the column is incomplete, even though only approximately 20% of the DBC determined with the single column experiment was used per switch.

Furthermore, even the fraction of lysozyme that did bind may not have been fully eluted because only two column void volumes were used for elution in zone I, whereas the single-column experiments required ten column void volumes to elute 90% of the lysozyme. A higher flow rate in zone I is necessary to ensure complete regeneration of the stationary phase, however, this would either require a higher flow rate in zone I, increasing back pressure and thus leakages, or a longer switching time, increasing analytical times and negating the aim of this study.

These results show that it is not feasible to perform SMB experiments with this setup under the given conditions (DBC, column back pressure, system tightness). Instead, a different continuous multi-column setup was tested by using a different valve stator. In this setup, each column operates independently in parallel for binding, washing, elution, and re-equilibration, minimizing total back pressure and leaks, allowing for higher flow rates in the single zones. This process features no countercurrent aspect like the more common PCC setup; however, the PCC setup relies on a long loading time in comparison to the time required for the other steps [29], which is not feasible due to the low DBC in combination with the long elution time of lysozyme.

Fig. 5(b) depicts the results of a CMCC run performed with the same zone I flow rate and feed flow rate as the SMB run depicted in Fig. 5(a).

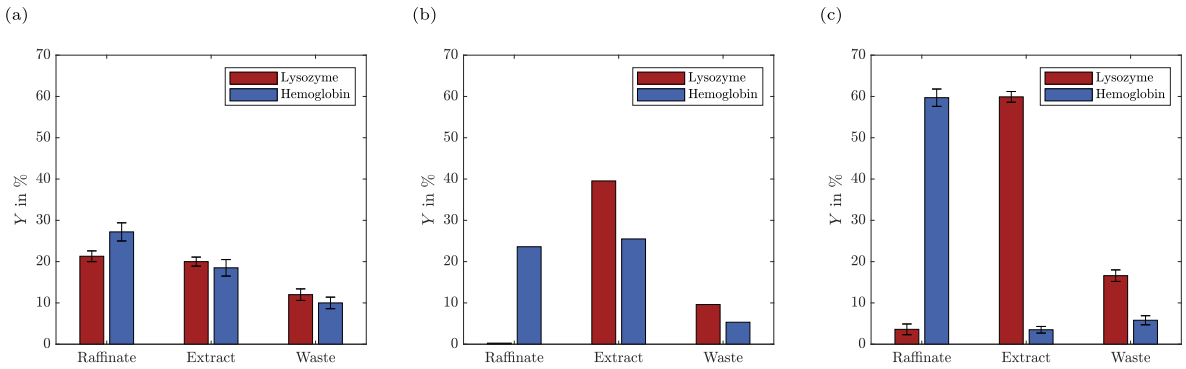

Fig. 5. (a) SMB experiment at pH 6.4 with a CVS of 2 in zone I; (b) CMCC experiment (CMCC 1) at pH 6.4 with a CVS of 2 in zone I; (c) optimized CMCC experiment (CMCC 5) at pH 8.2 with a CVS of 2.66 in zone I. Detailed process conditions for all runs are provided in Tables 1 and 2.

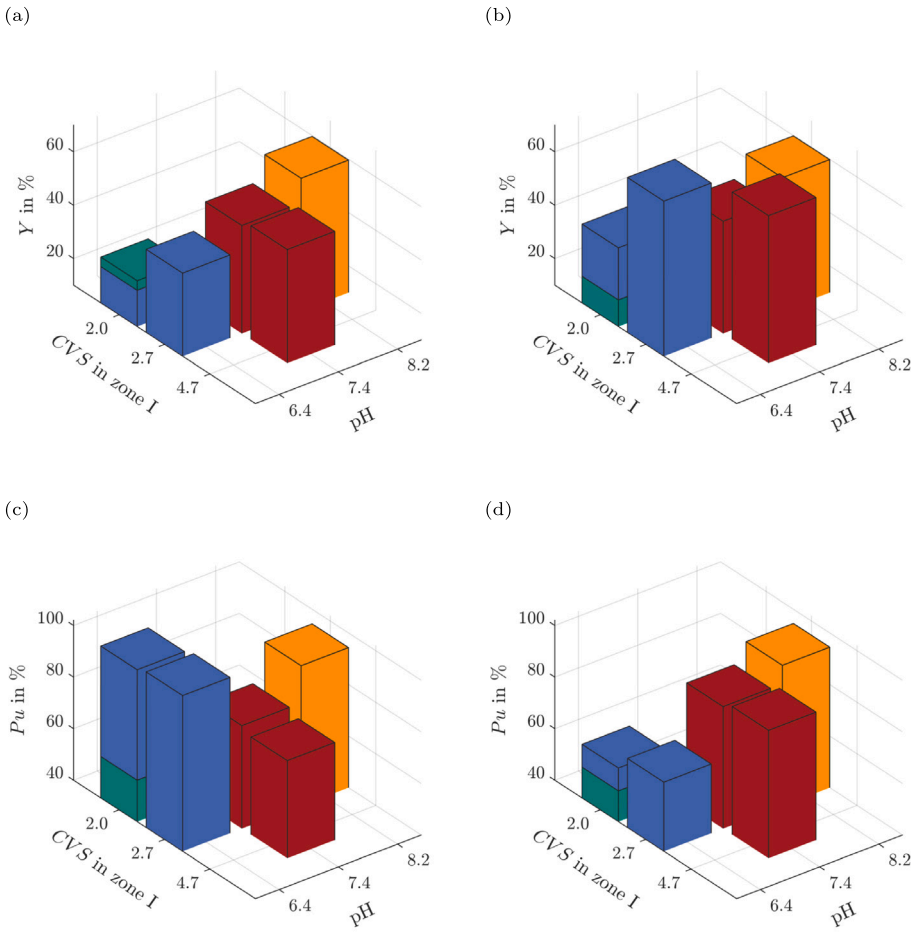

Fig. 6. Comparison of the SMB experiment with different CMCC runs in dependence of pH and CVS in zone I: (a) Hemoglobin yield in the raffinate; (b) lysozyme yield in the extract; (c) hemoglobin purity in the raffinate; (d) lysozyme purity in the extract. Green bars – SMB run, blue bars – CMCC runs at pH 6.4, red bars – CMCC runs at pH 7.4, orange bars – CMCC runs at pH 8.2. Detailed process conditions for all runs are provided in Tables 1 and 2. (For interpretation of the references to color in this figure legend, the reader is referred to the web version of this article.)

The flow rates of the wash and re-equilibration step were increased in comparison to the SMB run (compare Tables 1 and 2). The extract refers to the outlet of the elution step in this case, the raffinate is a pool of the feed and subsequent wash step and the waste is the output of the re-equilibration step. The purity of hemoglobin in the raffinate is greatly improved, indicating successful lysozyme binding. However, hemoglobin also partly binds to the stationary phase, decreasing both the hemoglobin yield in the raffinate and the extract purity. Also, only around 50% of lysozyme and hemoglobin were recovered with a volume balance of 86.4%, indicating that the elution is still incomplete.

Consequently, the flow rate in zone I was increased to enhance the elution process and the pH was increased to reduce hemoglobin binding. The results of a run were the pH was increased from 6.4 to 8.2 and the zone I CVS was increased from 2 to 2.66 is shown in Fig. 5(c). A volume balance of 90.9% (±3.2%, $n = 3$) was achieved under these conditions. The yield of both proteins was increased significantly to approximately 60%; the yield of the lysozyme in the extract could be increased further with a longer elution step, because more than 15% of the total lysozyme is recovered in the re-equilibration step. The purity of the extract is increased, since less hemoglobin bound to

the stationary phase at higher pH, however, the purity of the raffinate dropped slightly because more lysozyme did not bind at the higher pH.

Fig. 6 summarizes the yields and purities across different conditions. Fig. 6(a) shows the hemoglobin yield in the raffinate in dependence of CVS in zone I and pH. It indicates that the yield improves with higher pH values, as was expected since a higher mobile phase pH increases the difference to hemoglobin's isoelectric point, preventing its binding to the stationary phase. Literature values for the isoelectric point of hemoglobin range from 6.4–7.0 [30,31], though it can shift to more acidic values with increasing ionic strength of the buffer [30], or upon interacting with interfaces [31]. Consequently, only at a pH above 7 it can be ensured that the net charge of hemoglobin is negative independent of the respective conditions. At pH 6.4, a slight influence of the CVS in zone I can be observed, but not at pH 7.4. In theory, no influence of the CVS on the raffinate yield is expected for the non-binding hemoglobin.

Fig. 6(b) depicts the yield of lysozyme in the extract under the same conditions. The yield increases with higher CVS in zone I at pH 6.4 as well as 7.4. This was expected, since this results in a better elution, as discussed before. The dependence of the yield on the pH is not linear, the yield is lowest at a medium pH of 7.4. The pH influences the yield in two ways: A lower pH results in a better binding of the lysozyme to the column, resulting in less loss to the raffinate stream, while a higher pH probably results in a better elution of the protein, resulting in less loss due to incomplete elution. While at pH 6.4 and 8.2, the respective positive effects seem to outweigh the negative ones, pH 7.4 seems to combine those negative aspects, resulting in a lower yield.

This is also observable for the raffinate purity (Fig. 6(c)), where most lysozyme contaminates the raffinate stream at the medium pH of 7.4. At pH 8.2, the better elution results in the preservation of the DBC throughout the experiment, resulting in higher purities. As expected, no influence of the CVS in zone I is observable. Only a slight impact of the CVS in zone I on the extract purity is observable in Fig. 6(d), which is reasonable, since a longer elution step results in the elution of all bound protein. A significant influence of the pH on the extract purity is visible, showing that a pH of 6.4 is to low to prevent the binding of hemoglobin to the stationary phase.

Overall, these results show that the system is able to separate the proteins in CMCC mode. Although the purity and yield still are comparably low for both proteins, the results are encouraging for a first proof of concept, especially given the low DBC of this particular monolith.

4. Conclusion

This study showcases the limits of downscaling SMB using integrated monolithic capillary columns. The applied columns have a volume of 22 µL each and the valve stator has a channel volume of 24 µL in the case of SMB and 32 µL for the CMCC process. Under the given conditions, the stationary phase's low DBC and high back pressure did not permit the establishment of a suitable process point for SMB separations. The back pressure of a single monolith column with a length of 5 cm was approximately 3 bar at a flow rate of 50 µL/min, which prevented the connection of multiple chromatography columns in series. However, in a CMCC configuration using the columns in parallel, the setup successfully achieved protein separation with yields above 60% and purities above 80%. While these processes require further refinement, optimizing process parameters and improving monolith structure and functionalization, these findings underscore the potential of this system as a fast, continuous analytical tool with response times as short as 30 s for proteins recovered in the raffinate stream. The system was operated using the same set of columns for more than ten runs, totaling over 200 min of operation time and more than 400 valve switches, while maintaining consistent performance throughout.

Although valve tightness can be further improved, e.g., by evaluating different sealing materials or by employing an axial compression mechanism that applies more uniform pressure, this study demonstrates the valve's versatility: It shows how capillary columns can be integrated directly into the rotor and how exchanging only the stator enables different multi-column processes (SMB, CMCC) using the same set of columns, enabling the fast comparison of different processes. With these promising initial results, future studies should further explore the potential of combining advances in the miniaturization of single-column and multi-column processes, for example, by applying commercial high-pressure valves with a similar concept. This would enable the implementation of various continuous multi-column chromatography processes, such as SMB, at this scale, and allow the use of different types of capillary columns beyond monoliths, including particle-packed columns [32].

CRediT authorship contribution statement

Juliane Diehm: Writing – original draft, Visualization, Software, Methodology, Conceptualization. **David Achauer:** Writing – review & editing, Methodology, Investigation, Conceptualization. **Matthias Franzreb:** Writing – review & editing, Conceptualization.

Declaration of competing interest

The authors declare that they have no known competing financial interests or personal relationships that could have appeared to influence the work reported in this paper.

Acknowledgments

J.D. wants to thank the Cusanuswerk e.V. for the funding of her PhD scholarship.

Appendix A. Supplementary data

Supplementary material related to this article can be found online at https://doi.org/10.1016/j.chroma.2025.466245.

Data availability

Data will be made available on request.

References

[1] A. Jungbauer, Continuous downstream processing of biopharmaceuticals, Trends Biotechnol. 31 (8) (2013) 479–492, http://dx.doi.org/10.1016/j.tibtech.2013.05.011, URL https://www.sciencedirect.com/science/article/pii/S0167779913001200.

[2] A.S. Rathore, H. Agarwal, A.K. Sharma, M. Pathak, S. Muthukumar, Continuous processing for production of biopharmaceuticals, Prep. Biochem. Biotechnol. 45 (8) (2015) 836–849, http://dx.doi.org/10.1080/10826068.2014.985834, Publisher: Taylor & Francis _eprint: https://doi.org/10.1080/10826068.2014.985834.

[3] F. Feidl, S. Vogg, M. Wolf, M. Podobnik, C. Ruggeri, N. Ulmer, R. Wälchli, J. Souquet, H. Broly, A. Butté, M. Morbidelli, Process-wide control and automation of an integrated continuous manufacturing platform for antibodies, Biotechnol. Bioeng. 117 (5) (2020) 1367–1380, http://dx.doi.org/10.1002/bit.27296, URL https://onlinelibrary.wiley.com/doi/abs/10.1002/bit.27296, _eprint: https://onlinelibrary.wiley.com/doi/pdf/10.1002/bit.27296.

[4] L. Gerstweiler, J. Bi, A.P. Middelberg, Continuous downstream bioprocessing for intensified manufacture of biopharmaceuticals and antibodies, Chem. Eng. Sci. (2020) http://dx.doi.org/10.1016/j.ces.2020.116272.

[5] A. Jungbauer, P. Satzer, A. Duerauer, A. Azevedo, R. Aires-Barros, B. Nilsson, S. Farid, S. Goldrick, M. Ottens, M. Sponchioni, H. Marcelo Fernandez Lahore, Continuous downstream processing, Sep. Purif. Technol. 338 (2024) 126439, http://dx.doi.org/10.1016/j.seppur.2024.126439, URL https://www.sciencedirect.com/science/article/pii/S1383586624001783.

[6] J.K. Lorek, M. Isaksson, B. Nilsson, Chromatography in downstream processing of recombinant adeno-associated viruses: A review of current and future practises, Biotechnol. Bioeng. n/a (n/a) (2025) http://dx.doi.org/10.1002/bit.28932, URL https://onlinelibrary.wiley.com/doi/abs/10.1002/bit.28932, _eprint: https://onlinelibrary.wiley.com/doi/pdf/10.1002/bit.28932.

[7] M. Kornecki, A. Schmidt, L. Lohmann, M. Huter, F. Mestmäcker, L. Klepzig, M. Mouellef, S. Zobel-Roos, J. Strube, Accelerating biomanufacturing by modeling of continuous bioprocessing—Piloting case study of monoclonal antibody manufacturing, Processes 7 (8) (2019) 495, http://dx.doi.org/10.3390/pr7080495, URL https://www.mdpi.com/2227-9717/7/8/495, Number: 8 Publisher: Multidisciplinary Digital Publishing Institute.

[8] N. Andersson, J.G. Fons, M. Isaksson, S. Tallvod, D. Espinoza, L. Sjökvist, G.Z. Andersson, B. Nilsson, Methodology for fast development of digital solutions in integrated continuous downstream processing, Biotechnol. Bioeng. 121 (8) (2024) 2378–2387, http://dx.doi.org/10.1002/bit.28501, URL https://onlinelibrary.wiley.com/doi/abs/10.1002/bit.28501, _eprint: https://onlinelibrary.wiley.com/doi/pdf/10.1002/bit.28501.

[9] A.S. Rathore, G. Thakur, N. Kateja, Continuous integrated manufacturing for biopharmaceuticals: A new paradigm or an empty promise? Biotechnol. Bioeng. 120 (2) (2023) 333–351, http://dx.doi.org/10.1002/bit.28235, URL https://onlinelibrary.wiley.com/doi/abs/10.1002/bit.28235, _eprint: https://onlinelibrary.wiley.com/doi/pdf/10.1002/bit.28235.

[10] D.P. Wasalathanthri, R. Shah, J. Ding, A. Leone, Z.J. Li, Process analytics 4.0: A paradigm shift in rapid analytics for biologics development, Biotechnol. Prog. 37 (4) (2021) e3177, http://dx.doi.org/10.1002/btpr.3177, URL https://onlinelibrary.wiley.com/doi/10.1002/btpr.3177.

[11] A.S. Rathore, D. Sarin, S. Bhattacharya, S. Kumar, Multi-attribute monitoring applications in biopharmaceutical analysis, J. Chromatogr. Open 6 (2024) 100166, http://dx.doi.org/10.1016/j.jcoa.2024.100166, URL https://www.sciencedirect.com/science/article/pii/S2772391724000537.

[12] R.P. Faria, A.E. Rodrigues, Instrumental aspects of simulated moving bed chromatography, J. Chromatogr. A 1421 (2015) 82–102, http://dx.doi.org/10.1016/j.chroma.2015.08.045, URL https://linkinghub.elsevier.com/retrieve/pii/S0021967315012261.

[13] A. Seidel-Morgenstern, L.C. Keßler, M. Kaspereit, New developments in simulated moving bed chromatography, Chem. Eng. Technol. 31 (6) (2008) 826–837, http://dx.doi.org/10.1002/ceat.200800081, URL http://doi.wiley.com/10.1002/ceat.200800081.

[14] J. Diehm, L. Witting, F. Kirschhöfer, G. Brenner-Weiß, M. Franzreb, Micro simulated moving bed chromatography-mass spectrometry as a continuous online process analytical tool, Anal. Bioanal. Chem. (2023) http://dx.doi.org/10.1007/s00216-023-05023-9, URL https://link.springer.com/10.1007/s00216-023-05023-9.

[15] J. Diehm, T. Ballweg, M. Franzreb, Development of a 3D printed micro simulated moving bed chromatography system, J. Chromatogr. A 1695 (2023) 463928, http://dx.doi.org/10.1016/j.chroma.2023.463928, URL https://linkinghub.elsevier.com/retrieve/pii/S0021967323001541.

[16] J.P.C. Vissers, Recent developments in microcolumn liquid chromatography, J. Chromatogr. A 856 (1) (1999) 117–143, http://dx.doi.org/10.1016/S0021-9673(99)00692-5, URL https://www.sciencedirect.com/science/article/pii/S0021967399006925.

[17] L. Shan, B.R. Jones, Nano-LC: An updated review, Biomed. Chromatogr. 36 (5) (2022) e5317, http://dx.doi.org/10.1002/bmc.5317, URL https://onlinelibrary.wiley.com/doi/abs/10.1002/bmc.5317, _eprint: https://onlinelibrary.wiley.com/doi/pdf/10.1002/bmc.5317.

[18] P.S. Gomes, M. Zabkova, M. Zabka, M. Minceva, A.E. Rodrigues, Separation of chiral mixtures in real SMB units: The FlexSMB-LSRE®, AIChE J. 56 (1) (2010) 125–142, http://dx.doi.org/10.1002/aic.11962, URL https://onlinelibrary.wiley.com/doi/abs/10.1002/aic.11962, _eprint: https://onlinelibrary.wiley.com/doi/pdf/10.1002/aic.11962.

[19] S. Katsuo, C. Langel, P. Schanen, M. Mazzotti, Extra-column dead volume in simulated moving bed separations: Theory and experiments, J. Chromatogr. A 1216 (7) (2009) 1084–1093, http://dx.doi.org/10.1016/j.chroma.2008.12.031, URL http://www.sciencedirect.com/science/article/pii/S0021967308021961.

[20] D. Sýkora, F. Svec, J.M.J. Fréchet, Separation of oligonucleotides on novel monolithic columns with ion-exchange functional surfaces, J. Chromatogr. A 852 (1) (1999) 297–304, http://dx.doi.org/10.1016/S0021-9673(99)00004-7, URL https://www.sciencedirect.com/science/article/pii/S0021967399000047.

[21] M. Conti, J.A. Symington, J.R. Pullen, R. Mravljak, A. Podgornik, S. Dimartino, Porous platform inks for fast and high-resolution 3D printing of stationary phases for downstream processing, Adv. Mater. Technol. 8 (19) (2023) 2300801, http://dx.doi.org/10.1002/admt.202300801, URL https://onlinelibrary.wiley.com/doi/abs/10.1002/admt.202300801, _eprint: https://onlinelibrary.wiley.com/doi/pdf/10.1002/admt.202300801.

[22] H. Schmidt-Traub, M. Schulte, A. Seidel-Morgenstern, Preparative Chromatography, second ed., John Wiley & Sons, Ltd, 2012, http://dx.doi.org/10.1002/9783527649280, URL https://onlinelibrary.wiley.com/doi/10.1002/9783527649280, _eprint: https://onlinelibrary.wiley.com/doi/pdf/10.1002/9783527649280.

[23] M. Juza, M. Mazzotti, M. Morbidelli, Simulated moving-bed chromatography and its application to chirotechnology, Trends Biotechnol. 18 (3) (2000) 108–118, http://dx.doi.org/10.1016/S0167-7799(99)01419-5, URL https://linkinghub.elsevier.com/retrieve/pii/S0167779999014195.

[24] J. Diehm, V. Hackert, M. Franzreb, Configurable 3D printed microfluidic multiport valves with axial compression, Micromachines 12 (10) (2021) 1247, http://dx.doi.org/10.3390/mi12101247, URL https://www.mdpi.com/2072-666X/12/10/1247.

[25] T. Scientific, ProSwift ion-exchange monolith columns for protein analysis, 2025, URL https://assets.fishersci.com/TFS-Assets/CMD/Specification-Sheets/65843-DS-ProSwift-IEX-29Mar2010-LPN2020-02.pdf.

[26] Sartorius, CIMmultus® SO3 4 mL monolithic column (2 µm) | chromatography monoliths | sartorius eShop, 2025, URL https://shop.sartorius.com/de/p/cimmultus-so3-4-ml-monolithic-column-2-m/414.6157-2#.

[27] N.P. Dinh, Q.M. Cam, A.M. Nguyen, A. Shchukarev, K. Irgum, Functionalization of epoxy-based monoliths for ion exchange chromatography of proteins, J. Sep. Sci. 32 (15–16) (2009) 2556–2564, http://dx.doi.org/10.1002/jssc.200900243, URL https://onlinelibrary.wiley.com/doi/abs/10.1002/jssc.200900243, _eprint: https://onlinelibrary.wiley.com/doi/pdf/10.1002/jssc.200900243.

[28] E.G. Vlakh, T.B. Tennikova, Preparation of methacrylate monoliths, J. Sep. Sci. 30 (17) (2007) 2801–2813, http://dx.doi.org/10.1002/jssc.200700284, URL https://onlinelibrary.wiley.com/doi/abs/10.1002/jssc.200700284, _eprint: https://onlinelibrary.wiley.com/doi/pdf/10.1002/jssc.200700284.

[29] L. Gerstweiler, J. Bi, A.P. Middelberg, Continuous downstream bioprocessing for intensified manufacture of biopharmaceuticals and antibodies, Chem. Eng. Sci. 231 (2021) 116272, http://dx.doi.org/10.1016/j.ces.2020.116272, URL https://linkinghub.elsevier.com/retrieve/pii/S0009250920308046.

[30] H. Shirahama, K. Suzuki, T. Suzawa, Bovine hemoglobin adsorption onto polymer latices, J. Colloid Interface Sci. 129 (2) (1989) 483–490, http://dx.doi.org/10.1016/0021-9797(89)90462-1, URL https://www.sciencedirect.com/science/article/pii/0021979789904621.

[31] S. Devineau, K.-i. Inoue, R. Kusaka, S.-h. Urashima, S. Nihonyanagi, D. Baigl, A. Tsuneshige, T. Tahara, Change of the isoelectric point of hemoglobin at the air/water interface probed by the orientational flip-flop of water molecules, Phys. Chem. Chem. Phys. 19 (16) (2017) 10292–10300, http://dx.doi.org/10.1039/C6CP08854F, URL https://pubs.rsc.org/en/content/articlelanding/2017/cp/c6cp08854f, Publisher: Royal Society of Chemistry.

[32] Y. Liu, H. Wen, S. Chen, X. Wang, X. Zhu, L. Luo, X. Wang, B. Zhang, Mass fabrication of capillary columns based on centrifugal packing, Anal. Chem. 94 (23) (2022) 8126–8131, http://dx.doi.org/10.1021/acs.analchem.2c00442, Publisher: American Chemical Society.